REGULAR PAPER

Ankle Foot Orthosis for Patients with Drop Foot Using Shape-Memory-Alloy Actuators

Bohyun Lee[1] · Ji Su Park[1] · Shinsuk Park[2] · Choong Hyun Kim[1]

Abstract

Gait disorders can lower the quality of life of patients. Drop foot, a causative factor of deviated gait patterns, renders patients unable to lift their forefoot towards the body. Hence, a light and compact ankle–foot orthosis (AFO), which is the most common treatment for drop foot, must be designed, especially for patients with impaired lower limb muscles as oxygen consumption increases by 30% per 1.96 N load on their foot. Furthermore, the limited range of ankle angles in the first 10% of the gait cycle (GC) is a major drawback for patients with drop foot compared to healthy individuals. This limited range of ankle angles can be improved by gaining support from an AFO composed of shape memory alloy (SMA) actuators (SMA-AFO). Therefore, in this study, an SMA was used to fabricate a soft actuator to reduce the weight of the AFO. An adaptive frequency oscillator (AO) was implemented in real time for continuous gait phase detection. Walk tests were performed on a treadmill with the SMA-AFO attached to the participants (N = 3). The experimental results showed that the participants could lift their forefoot in the dorsiflexion direction with an ankle angle of 8.75° in the first 10% of the GC. Furthermore, the current required to operate the SMA actuator can be supplied to only 45.3% of the GC, reducing the power consumption. Therefore, the proposed SMA-AFO can be used in patients with drop foot.

Keywords Ankle foot orthosis · Shape memory alloy · Actuator · Adaptive frequency Oscillator · Gait disorder · Gait phase detection · Drop foot · Gait assistance

1 Introduction

Walking is the most basic human activity of daily living, and walking characteristics serve as criteria for determining the health of individuals [1]. Therefore, gait disorders significantly reduce the quality of life of patients [2]. The major causes of gait disorders include myelopathy, Parkinson's disease, stroke, and cerebellar atrophy [3, 4]. Stroke, one of the causes of gait disorders, leads to an unstable gait pattern, with patients showing the "drop foot" phenomenon due to lower motor neuron disease, which prevents the forefoot from being pulled towards the body during walking. Patients with drop foot lose their postural stability during the stance phase of gait because the forefoot and outer edge of the foot become overloaded, making it difficult to support their weight with the affected foot. Consequently, the sequelae of drop foot place patients at risk of falling [4, 5]. Carolus et al. reported that 69% of patients with drop foot required mobility aids when walking [6].

Ankle–foot orthoses (AFOs) are the most commonly used mobility aids for patients with drop foot [7]. AFOs can be categorized according to actuator types: series elastic actuator (SEA), hydraulic actuator, pneumatic actuator, and etc. Blaya et al. developed an AFO with SEA to improve foot slap and toe drag of drop foot patients [8]. The study showed a reduced frequency of slap foot and normal-like ankle kinematics in the swing phase with a variable impedance control [8]. Noël et al. proposed an AFO with a hydraulic actuator and an electric motor which could offer a decent quality of force and position control [9]. PID control was implemented

✉ Choong Hyun Kim
nems.kim@gmail.com

Bohyun Lee
bohyun505@gmail.com

Ji Su Park
indicepark@gmail.com; drsspark@korea.ac.kr

1   Center for Bionics, Korea Institute of Science and Technology, 5, Hwarang-Ro 14-Gil, Seongbuk-Gu, Seoul 02792, Republic of Korea

2   Department of Mechanical Engineering, Korea University, Seoul 02841, Republic of Korea

and the developed device can operate in two different directions, tension and compression [9]. For the pneumatic actuator type, an AFO with a bidirectional pneumatic rotary actuator was introduced by Shorter et al. The device assists in two directions: plantarflexion and dorsiflexion. Decreased muscle activation of the tibialis anterior was observed during stance and swing phase on able-bodied subjects [10]. Another study on an AFO using a pneumatic actuator was performed by Choi et al. In this study, pneumatic artificial muscles were fabricated to actuate an AFO, and the device offered two degree-of-freedom, inversion and eversion of an ankle, unlike most AFOs [11]. However, as oxygen consumption increases by 30% when the load applied to the foot increases by 1.96 N, designing a lightweight and compact AFO for these patients is essential [12]. Especially, the metabolic cost of walking increases proportionally to the load on the distal position on a human body such as extremities [13]. Therefore, it is important to minimize the load of an AFO part located on a foot.

The weights of AFOs located on a lower extremity developed by Choi et al. [11] and Shorter et al. [10] are 1.44 kg and 1.9 kg, respectively, making them rather heavy to use by patients with walking disabilities. Therefore, it is necessary to reduce the AFO weight by adopting another type of an actuator such as a soft actuator [14].

A shape memory alloy (SMA), a representative soft actuator, can be used for this purpose. SMAs have the property of returning to the previously memorized shape when heated and have been applied as actuators for various devices including AFOs because of their relatively high output performance for their weight [15].

Pittaccio et al. used SMA wire-based actuators fixed on the shin and foot for the post-stroke rehabilitation [16]. It was shown that the developed device could produce the minimum range of motion for dorsiflexion [16]. Zhang et al. developed a robotic ankle–foot with an artificial skeletal muscle-like SMA actuator that was capable of actuating, energy-storing and self-sensing. The device was able to accurately follow the desired angle but the low bandwidth (approx. 0.17 Hz) of the actuator was the difficulty to overcome due to the slow heat-transfer rate of SMA [17]. Deberg et al. applied superelastic SMA wires with small pulleys to a passive ankle foot orthosis. The developed device resulted in an improved dorsiflexion of a drop foot patient compared to a conventional passive AFO [18].

Agostini et al. [19] analyzed the gait phase using three foot switches and divided the gait cycle (GC) into four types: heel contact (H), flat foot contact (F), push-off or heel-off (P), and swing (S), as shown in Fig. 1. Most healthy adults showed a GC of H-F-P-S, as illustrated in Fig. 1a, whereas some patients with drop foot showed a GC of P-F-P-S, as depicted in Fig. 1b [19]. This unstable gait pattern can be interpreted as the appearance of the P phase instead of the H phase because the
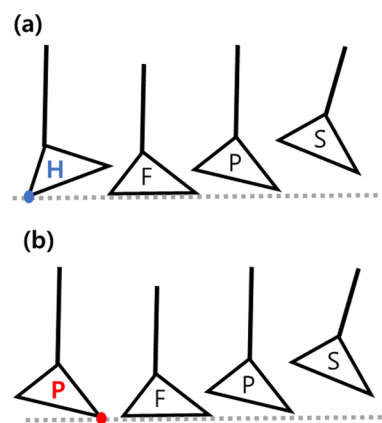

Fig. 1 Gait patterns of **a** healthy participants and **b** patients with drop foot: H, heel contact; F, flat foot; P, push-off; S, swing [19]

drop foot leads the forefoot to contact the ground in the initial phase, where heel contact occurs. Wisszomirska et al. [20] and Blazkiewicz et al. [21] reported that the range of motion (ROM) for the motion of lifting the instep towards the shin (dorsiflexion [DF]) in patients with drop foot was the most limited in the initial 0%–10% of the GC. In this gait phase, the ankle angle of these patients was approximately 8° lower than that of healthy adults. Knee hyperextension occurs as a compensatory mechanism when ankle movement is restricted during walking, which makes it impossible for the knee joint to support the weight of the patient, leading to difficulties in walking normally [20]. Therefore, identifying the initial 0%–10% of the GC and increasing the ankle angle by approximately 8° is essential when assisting the gait of patients with drop foot using an AFO.

Therefore, in this study, we performed the following experiments to develop and test an AFO using SMA as actuators (SMA-AFO) to solve these problems. Firstly, a control method suitable for the SMA characteristics was developed after identifying the behavioral characteristics of the SMA. Secondly, the GC was identified using gait phase detection, which could be applied even when an AFO is worn while using the ground reaction force (GRF) as input. Thirdly, a control method for the SMA-AFO that could maximize the gait assistance effect for patients with drop foot while minimizing the operation period of the SMA according to the GC was proposed, and the performance of the SMA-AFO was analyzed using a walk test.

2 Device and Methods

2.1 Construction of SMA-AFO

The SMA-AFO developed in this study consists of an AFO divided into upper and lower parts around a hinge that

accommodates the rotation of the ankle joint; two SMA actuators that are fixed on the upper and lower parts of the AFO and lift the lower part of the AFO towards the shin; an SMA controller that identifies the GC and controls the operation of the SMA actuators; and an insole device that measures the GRF and detects the gait phase (Fig. 2). Furthermore, a rotary angle sensor (SV01A103AEA01, Murata Manufacturing Company, Kyoto, Japan) was installed on the hinge of the ankle joint, which is a component of the AFO (Fig. 6), to measure and analyze changes in the ankle angle during walking.

The SMA actuator is an artificial muscle that operates under the principle that force is generated by the contraction of muscle fibers, and the force exerted during this function is proportional to the contraction strain of the artificial muscle. Although the contraction strain of an SMA wire is less than 10%, it increases to approximately 50% when the SMA spring is composed of an SMA wire [22, 23]. Therefore, in this study, springs composed of SMA wires were used as actuators to play the role of the tibialis anterior, which is the muscle responsible for ankle DF.

The contraction strain of the SMA spring is shown in Eq. (1) [22]:

$$\text{contraction strain}(\%) = \frac{\delta}{l_0} \times 10. \tag{1}$$

In Eq. (1), δ and l_0 are the contraction displacement and initial length of the SMA spring, respectively.

Furthermore, Park et al. [24] evaluated the force exerted by an SMA spring using the spring index (C) of the SMA spring. The design factors of the spring are shown in Fig. 3 where D_o and D_i are the outer and inner diameter of a spring, respectively. The spring diameter (D) is defined as the midpoint between D_o and D_i [25]. The spring index was
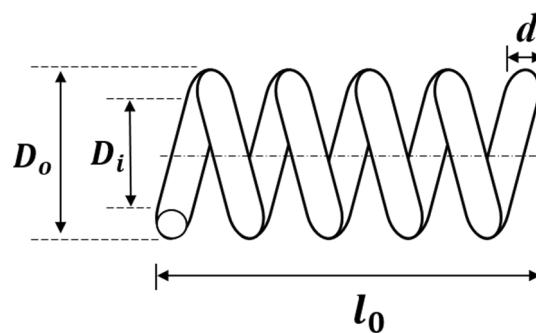

Fig. 3 SMA spring

calculated as the ratio of the D to the wire diameter (d), as expressed in Eq. (2):

$$C = \frac{D}{d}. \tag{2}$$

Referring to a previous study [24], the spring index of the SMA spring fabricated in this study was set to 6 to maintain a relatively constant displacement, even when the actuating frequency changed.

2.1.1 Fabrication of the SMA Spring

Figure 4 depicts the jig used to fabricate the SMA spring and the final fabricated SMA spring; the main specifications of the fabricated SMA spring are listed in Table 1. The fabrication process of the SMA spring can be described as follows. The SMA wire (Nitinol SMA muscle wire, Nexmetal Co., Alta Loma, California, U.S.A.) was firstly wrapped around the outside a 2.5-mm-diameter steel rod to maintain close contact between the wire turns, with the initial length of the SMA spring set at 60 mm and both ends fixed (Fig. 4b). The spring was then placed in an electric furnace (PMF-3, LAB House, Pocheon, Republic of Korea) and heat treated at 350 °C for 30 min for the SMA to memorize the shape of the spring (Fig. 4c). The final fabricated SMA spring is shown in Fig. 4d.

2.1.2 Composition of the SMA Actuator

Figure 5a provides a schematic of an SMA actuator. A total of 10 SMA spring sets consisting of two 60-mm-long SMA springs connected in series were manufactured, and both ends of each spring set were tied to terminals and fixed to an acrylic support with bolts, as shown in Fig. 5c. To the SMA spring set connected in this manner, electricity was supplied by configuring a circuit, as depicted in Fig. 5b. Insulation covers composed of a Teflon-coated high-temperature fabric (TBS-260, Alphaflon, Seoul, Republic of Korea) were used to cover the surfaces of each SMA spring and separate them
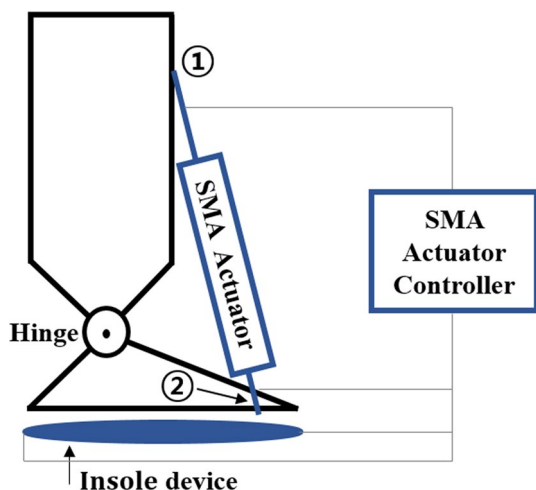

Fig. 2 Schematic of the developed SMA-AFO system

Fig. 4 SMA spring fabrication. **a** Spring fabrication jig, **b** SMA spring, **c** springs in the furnace (350 °C for 30 min), and **d** fabricated SMA springs
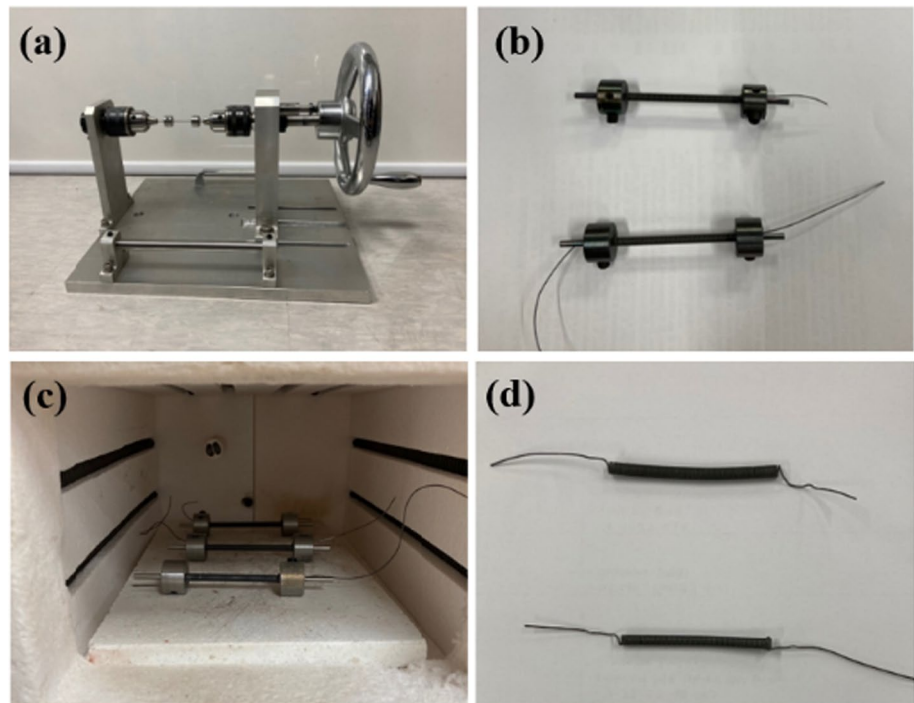

Table 1 Specifications of the SMA spring

Parameter	Value
SMA wire diameter (d)	0.5 mm
SMA spring diameter (D)	2.5 mm
Spring index (C)	5
Transition temperature	40 °C
Initial length (l_0)	60 mm

from one another, as shown in Fig. 5d), to prevent short circuits that could be caused by contact between adjacent SMA springs [26].

Two sets of SMA actuators were manufactured and installed on each side of the AFO, as shown in Fig. 6. Two bias springs were attached to the acrylic supports at the bottom of the SMA actuators to connect them to the lower part of the AFO. The bias springs ensure that tension always acts on the SMA actuators, even under any change in the length of the SMA springs, which enables smooth control of the movement of the SMA springs.

2.1.3 Characteristics of the SMA Actuator

To characterize the SMA actuator, deadweights were hung from the bottom of the SMA actuator, as depicted in Fig. 7. The change in length due to contraction of the SMA actuator, along with the change in dead weight, was measured while supplying current to the SMA spring sets using a direct current (DC) power supply (TDP-3030B, Toyotech,

Incheon, Republic of Korea). Subsequently, the spring constant of the SMA actuator was obtained from the data. Two voltage conditions, 12 V and 24 V, were selected for the DC power. Nine dead weights were used in the experiment (0.98, 2.94, 4.9, 6.86, 9.8, 11.76, 14.7, 16.66, and 19.6 N), and the experiment was repeated 10 times for each weight condition.

During the performance test of the SMA actuator, the temperatures of the outer surface of the insulation cover and surface of the SMA spring inside the cover were measured and observed using an infrared thermometer (VT04, Fluke Co., Everett, Washington, U.S.A.) and thermocouple (MAX6675, Maximum Integrated, San Jose, California, U.S.A.), respectively.

2.1.4 Location of the SMA Actuator on the AFO

To control the SMA-AFO efficiently, the location for installing the SMA actuators must be optimized. The ankle angles before and after operation of the SMA actuators are shown in Figs. 8a and b, respectively. For the foot and leg sizes applied to the AFO design, anthropometric data for South Korean men in their 60s, who have the highest stroke prevalence among South Koreans, were used [27, 28]. The origin (0,0) of the coordinate axis was based on the heel when designing the AFO. Table 2 lists the parameters and definitions related to location selection of the SMA actuator [27].

The torque (T) applied to the ankle by the SMA actuator can be obtained using the displacement ($\Delta \ell$) of the SMA actuator and the moment arm (r′). First, when the ankle is
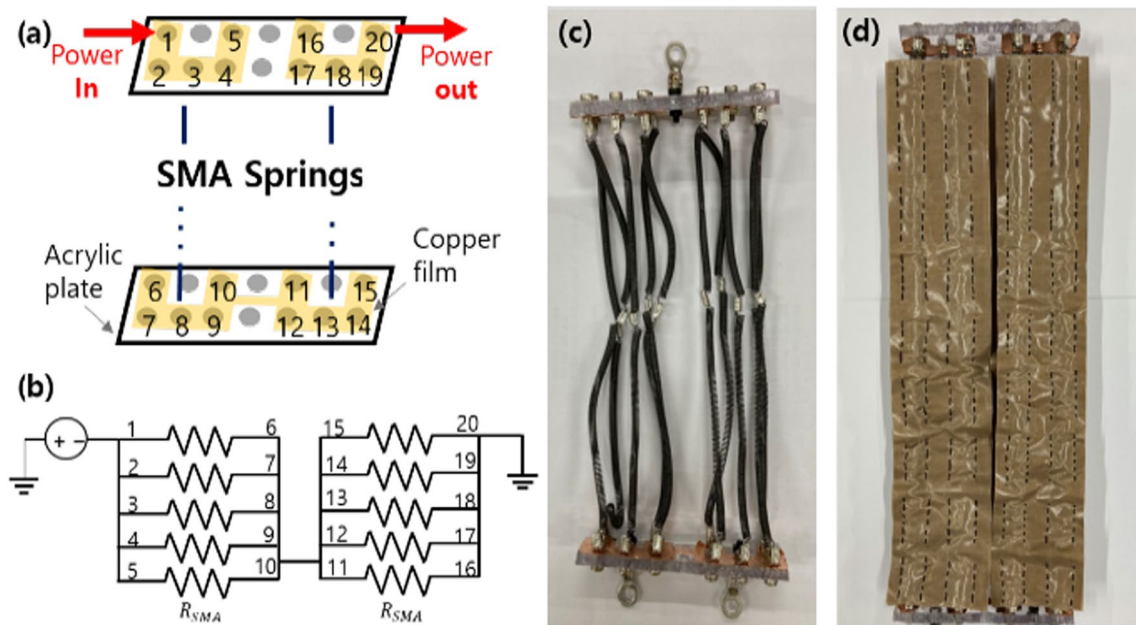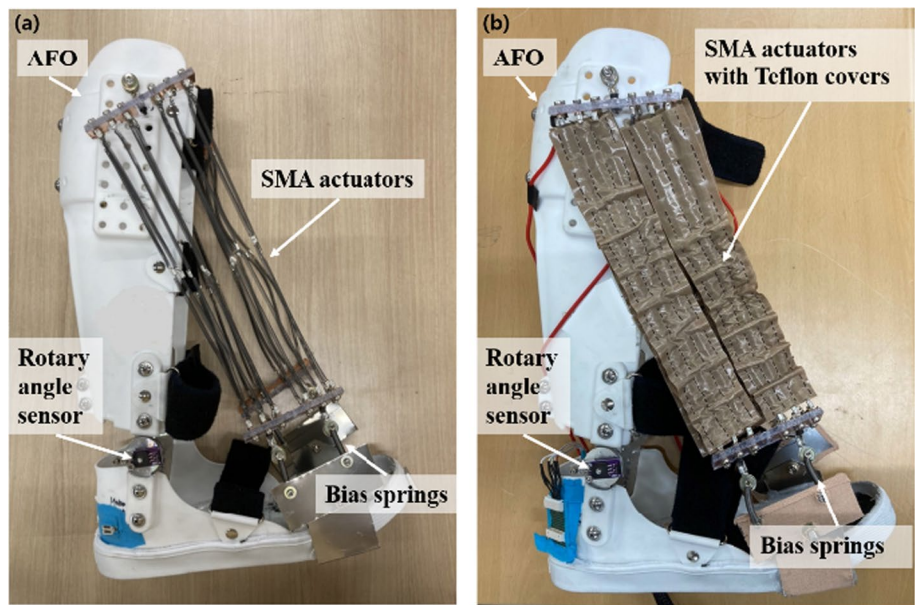
Fig. 5 Fabricated SMA actuator. **a** Schematic of the SMA actuator, **b** circuit of the SMA actuator system, **c** fabricated SMA actuator, and **d** fabricated SMA actuator with covers

Fig. 6 Overview of the SMA-AFO **a** without covers and **b** with Teflon-coated covers

dorsiflexed from a neutral state, the displacement of the actuator ($\Delta\ell$) is given as follows:

$$\Delta\ell = \ell - \ell'. \tag{3}$$

In Fig. 8b, if the fixed position of the actuator on the upper part of the AFO is (a, b), and the fixed position of the actuator on the lower part of the AFO is (c, d) with the contracted SMA actuator, the moment arm (r') can be obtained using Eq. (4):

$$r' = \frac{\left|(d-b)C_x + (a-c)C_y + (bc-ad)\right|}{\sqrt{(d-b)^2 + (a-c)^2}}. \tag{4}$$

The spring constant of the SMA spring obtained from the performance test in Sect. 2.1.3 was 0.33 N/mm, and the torque (T) of the SMA actuator assisting the DF was calculated as follows:

$$T = 0.33 \times \Delta\ell \times r'. \tag{5}$$

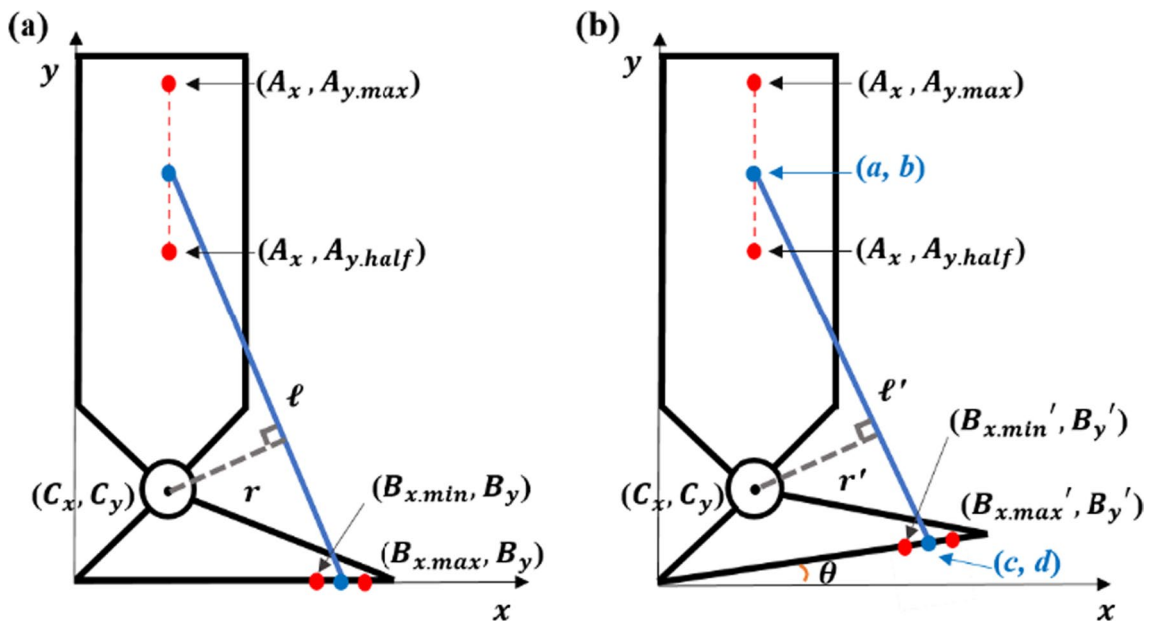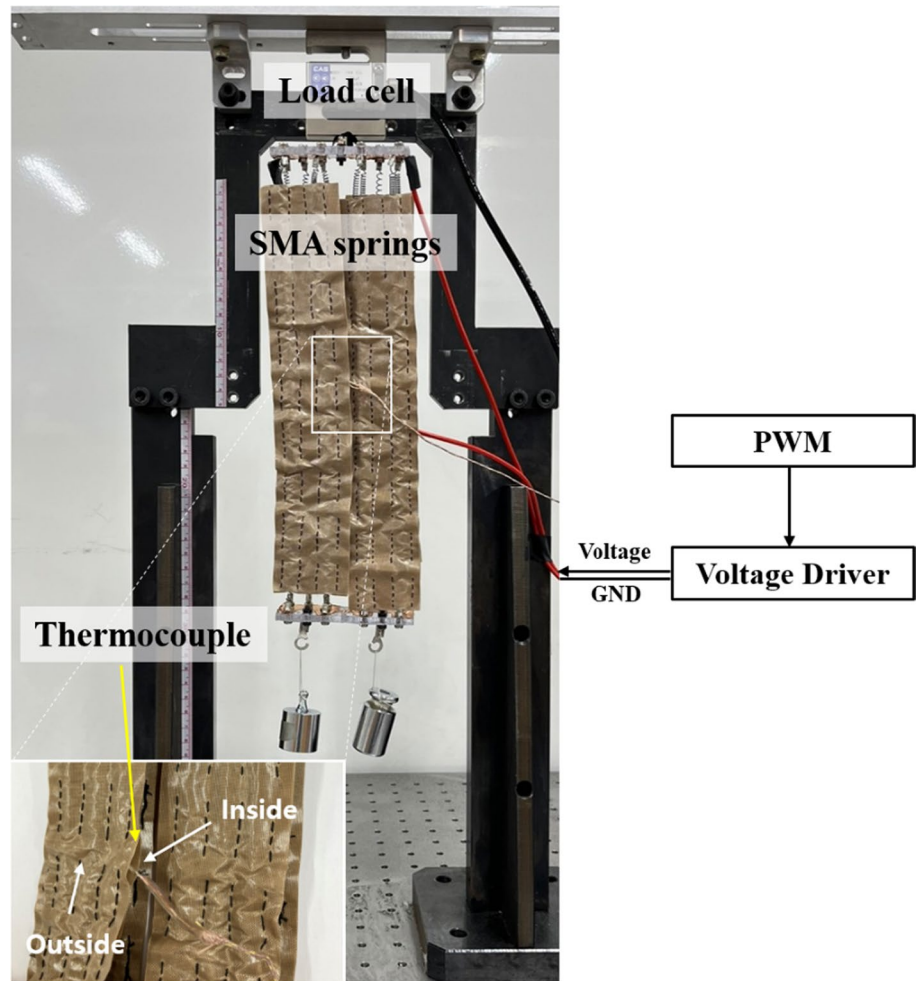**Fig. 7** Experimental setup configuration for testing the SMA actuator

Fig. 8 Schematic of the AFO at **a** neutral and **b** target-assistive angles

Table 2 Parameters and definitions for the design of an SMA-AFO

Parameter	Definition	Value
A_x	Ankle width×0.5	46.6 mm
$A_{y.half}$	Ay.max×0.5	191.2 mm
$A_{y.max}$	Heel–popliteal fossa	382.4 mm
$B_{x.min}$	Heel–instep	151.9 mm
$B_{x.max}$	Heel–little toe	208.5 mm
B_y	Ground	0 mm
C_x	Heel–lateral malleolus	36.4 mm
C_y	Height of the lateral malleolus	77.3 mm
θ	Ankle angle	–
θ_Δ	Δ Ankle angle	–
θ_t	Target assistive angle	8°

2.2 Detection of the Continuous Gait Phase

2.2.1 Adaptive Frequency Oscillator

Gait phase information is required to accurately assist the gait of the AFO wearer [29]. The most basic method of detecting the gait phase is to divide a GC into discrete phases such as the loading response (LR), mid-stance (MS), and initial swing (IW). However, controlling the AFO continuously is difficult owing to time delays [30].

In contrast, continuous gait phase detection has a relatively small time delay compared to the classification of the discrete phase, which enables smoother gait assistance and gait analysis [30]. An adaptive frequency oscillator (AO), which is an algorithm applied to detect the continuous gait phase, implements a Fourier function to receive data related to human body motion, such as the angle of the hip joint or the GRF, and calculates the frequency and amplitude to estimate the gait phase.

Park et al. [31] detected the continuous gait phase using GRF data collected by an insole device as the input data for the AO. Because this method can be applied not only to healthy adults, but also to patients with gait disorders who have abnormal changes in the GRF during walking, it was applied in this study. After placing each insole equipped with force-sensitive resistors (FSRs) on the sole of the AFO and shoe, the GRF signals were collected to calculate the center of pressure (COP) of the body. The gait phase was continuously detected by applying the medial–lateral COP, COPx, to the AO algorithm. The conceptual diagram of the AO used in this study is shown in Fig. 9, and the GC was obtained using Eqs. (6) – (11).

$$\dot{\varphi}_i(t) = i\omega(t) + k_\varphi e(t)cos\left(\varphi_i(t)\right) \tag{6}$$

$$\dot{\omega}(t) = k_\omega e(t)cos\left(\varphi_1(t)\right) \tag{7}$$
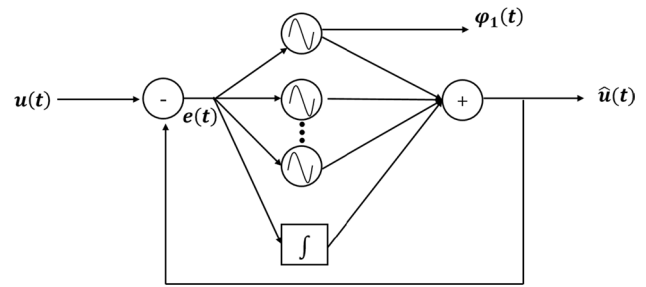

Fig. 9 Block diagram of the AO system

$$\dot{\alpha}_i(t) = k_\alpha e(t)sin\left(\varphi_i(t)\right) \tag{8}$$

$$\dot{\alpha}_0 = k_0 e(t) \tag{9}$$

$$\hat{u}(t) = \alpha_0(t) + \sum \alpha_i(t)sin(\varphi_i(t)) \tag{10}$$

$$e(t) = u(t) - \hat{u}(t) \tag{11}$$

In the above equations for the AO, α_i and φ_i are the amplitude and phase of the ith oscillator, respectively, and α_0 is the non-oscillating component. ω represents the fundamental frequency of the input, and $\hat{u}(t)$ is the signal learned through AO. The AO used in this study was designed using a sixth-order equation (i=6), where φ_1, the first signal frequency of $\hat{u}(t)$, is a low-frequency component of the input signal. φ_1 is evaluated to coincide with the GC in gait phase detection using the AO. Therefore, φ_1 is used as a GC value, and it varies between 0 and 2π. The point at which φ_1 became 0 was defined as the point at which COPx, used as an input signal in this study, changed from a negative value to a positive value.

COPx can be calculated as shown in Eq. (12):

$$COPx = \sum_{i=1}^{10} FSR_i \times x_i / \sum_{i=1}^{10} FSR_i, \tag{12}$$

where i is defined as the position of the FSRs placed on both feet, and the position defined in previous studies was used [32]. Figure 10 and Table 3 present the locations of the FSRs.

2.2.2 Control Strategy for the SMA Actuator

As it takes time for the SMA actuator to contract fully after supply of power, current must be supplied to the SMA actuator in advance from the previous GC to lift the lower part of the SMA-AFO such that the forefoot does not touch the ground in the 0–10% section of the GC.

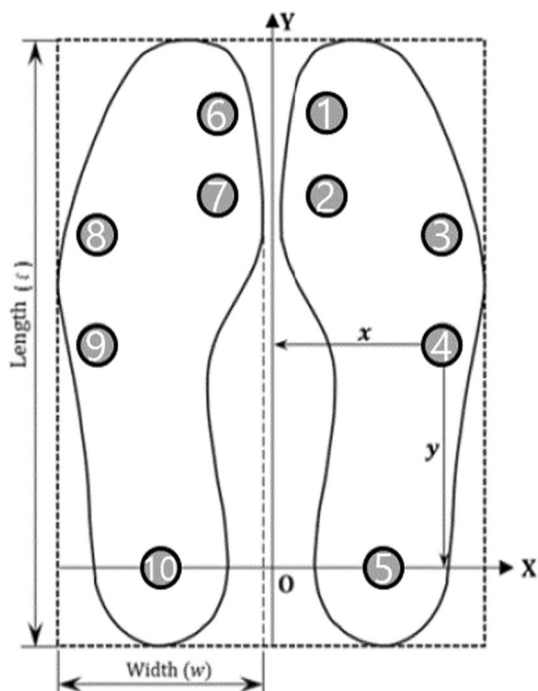The average time for the lower part of the SMA-AFO to rotate by approximately 8° towards the shin ($t_{cont.8°}$) was

Fig. 10 Locations of FSR sensors

Table 3 Locations of FSR sensors [32]

Sensor No	Foot side	Sensor position	X	Y
1	Right	Toe	$0.191H \times 0.5 - 0.25w$	$l_f \times 0.85$
2		First metatarsal	$0.191H \times 0.5 - 0.25w$	$l_f \times 0.73$
3		Fifth metatarsal	$0.191H \times 0.5 + 0.25w$	$l_f \times 0.64$
4		Cuboid	$0.191H \times 0.5 + 0.25w$	$l_f \times 0.50$
5		Heel	$0.191H \times 0.5$	$l_f \times 0.15$
6	Left	Toe	$-0.191H \times 0.5 + 0.25w$	$l_f \times 0.85$
7		First metatarsal	$-0.191H \times 0.5 + 0.25w$	$l_f \times 0.73$
8		Fifth metatarsal	$-0.191H \times 0.5 - 0.25w$	$l_f \times 0.64$
9		Cuboid	$-0.191H \times 0.5 - 0.25w$	$l_f \times 0.50$
10		Heel	$-0.191H \times 0.5$	$l_f \times 0.15$

Height, H; foot length $l_f = 0.152 \times H$; and foot width w $= 0.055 \times H$, units in mm

approximately 1.7 s once current was supplied to the SMA actuator when the experiment was repeated 10 times. When a participant walks a stride of 600 mm at 0.15 m/s, the time required for one stride ($t_{1stride}$) is 4 s, and the ratio of the time required to rotate the ankle by 8° to the total GC corresponds to 42.5% ($t_{cont.8}$/$t_{1stride}$).

According to Park et al. [32], as shown in Fig. 11, the IW, mid-swing (MW), terminal swing (TW), and LR of the next GC account for approximately 45.3% of the total time required for one-stride walking. As this ratio was approximately 1.07 times more than the ratio of $t_{cont.8}$/
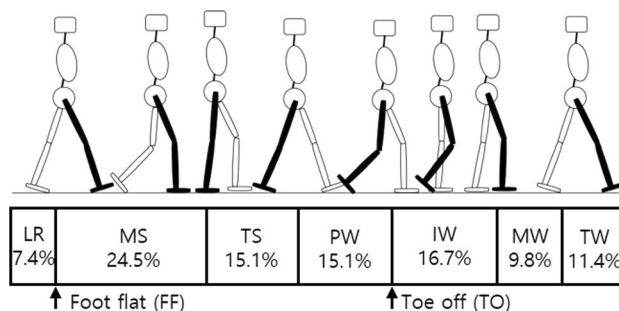

Fig. 11 Gait phase detection for controlling the SMA actuator using the GC given by Park et al. [32]

$t_{1stride}$ (42.5%), these two ratios were considered similar in this study, and we decided to control the SMA actuators by supplying power in this section of the GC. In other words, the SMA spring must contract sufficiently to assist the DF in the 0–10% section of the GC, and the time required for the SMA actuator to contract fully was approximately 45% of the GC. The strategy was to start supplying power at the start of the IW, which was approximately 45% before the end of the LR, and to stop supplying power at the end of the LR, where the starting point of the IW corresponded to the point at which the toes were away from the ground (toe off [TO]). The LR endpoint corresponded to the point at which the sole was parallel to the ground (foot flat [FF]). The FF and TO were defined as the times at which FSR #1 on the sole of the SMA-AFO touched the ground, the load value increased, and the load value decreased after leaving the ground.

2.3 Participants

A total of three healthy adults, two males (mean age, 32.5 years; mean weight, 73 kg; and mean height, 1.73 m) and one female (age, 25; weight, 54 kg; height, 1.64 m), participated in the walk test using the SMA-AFO.

2.3.1 Experimental Method

As shown in Fig. 12, the participants wore the SMA-AFO developed in this study on their right foot and walked on a treadmill (M-gait, Motek, Amsterdam, Netherlands) with a 600 mm stride at a walking speed of 0.15 m/s. According to the study by Bogataj et al., the mean gait speed of patients suffering from severe hemiplegia due to cerebrovascular accident (stroke) was 0.19m/s, and the average age of this group was 59.1, which could be considered to be close to the age of 60 [33]. This group could be regarded as the representative of our study's target since the drop foot is one of the most common secondary conditions by hemiplegia [34]. Therefore, the walking speed for the experiment in this study was set based on the reference.

A fire-retardant fabric with a thickness of 5 mm was placed on the right shin of each participant, and the SMA-AFO was worn to prepare for the case in which the surface of the SMA actuator was exposed to high temperatures.

For the walk test, experiments were conducted in the following order as shown in Fig. 13. Healthy adult participants imitated and practiced the gait pattern of a patient with drop foot, the above-described GC of P-F-P-S, for about five minutes and then imitated it during the whole test. The first set of walk tests was conducted with inactive SMA actuators. Each participant walked on the treadmill for 2 min and took a one-minute break per trial for a total of two trials. After a three-minute rest period, the second set of walk tests was performed with active SMA actuators. Each participant started walking with inactive SMA actuators for the first 40 s, then the SMA actuators were activated for 40 s. After that, the SMA actuators were inactivated for the next 40 s for one trial (Fig. 14). A total of five trials were repeated per subject. For the second set of walk tests, data collected with the activated SMA actuators for 40 s per trial was used for the comparison of the ankle angle. Each trial was conducted after confirming that the SMA actuators were sufficiently cooled.
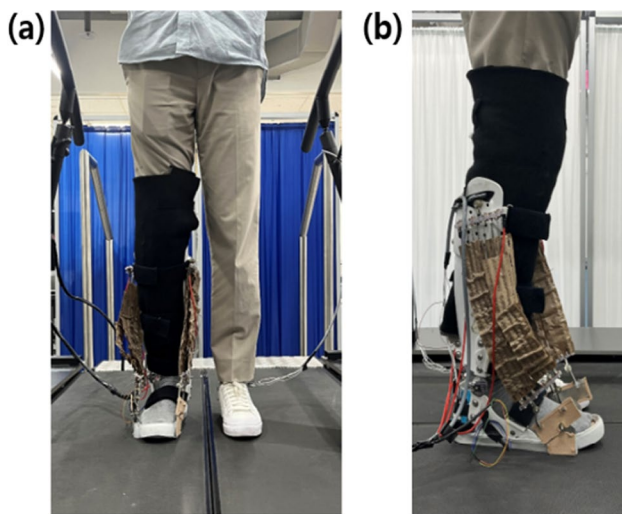

Fig. 14 Schematic of the walk test

2.4 Statistical analysis

To test the normality of data, Shapiro–Wilk test was conducted using Excel 2016. The Shapiro–Wilk test statistic was calculated by using Eq. (13):

$$W = \frac{\left(\sum_{i=1}^{n} a_i x_{(i)}\right)^2}{\sum_{i=1}^{n} (x_i - \bar{x})^2} \tag{13}$$

where x_i are the ordered sample values, $\bar{x}$ is the sample mean, and a_i are constants [35].

The paired t-test was used to compare the ankle angle difference under using inactive and active SMA actuators. Statistical analysis was performed using MATLAB (version 9.8.0.1323502, R2020a) with a significant p-value of 0.05.

3 Results and Discussion

3.1 Characteristics of the SMA Actuator

Table 4 lists the experimental results for the active SMA actuators with two types of input voltages (12 V and 24 V). When a dead weight of 19.6 N was suspended on the SMA actuator and input voltages of 12 V and 24 V were supplied, the changes in the length of the SMA actuator were 60 mm and 58 mm, respectively, showing a difference of 2 mm. The time required for the SMA actuator to contract fully under the 12 V and 24 V conditions was 23 s and 1.7 s, respectively, which differ by 21.3 s. The temperature of the SMA actuator was found to increase up to 227 °C with the input voltage of 24 V, which is more than double of the temperature when the input voltage was 12 V. Overall, there is no significant differences in the displacement of the SMA actuator under the two different input voltage conditions. However, the time required for the SMA actuator to contract

Fig. 12 Setup of the walk test. **a** Participant on Motek M-gait treadmill and **b** participant wearing the SMA-AFO with fire-retardant fabric on the right leg
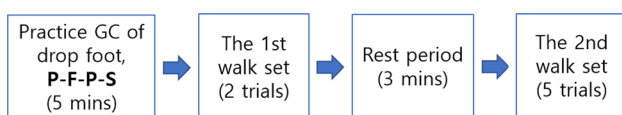

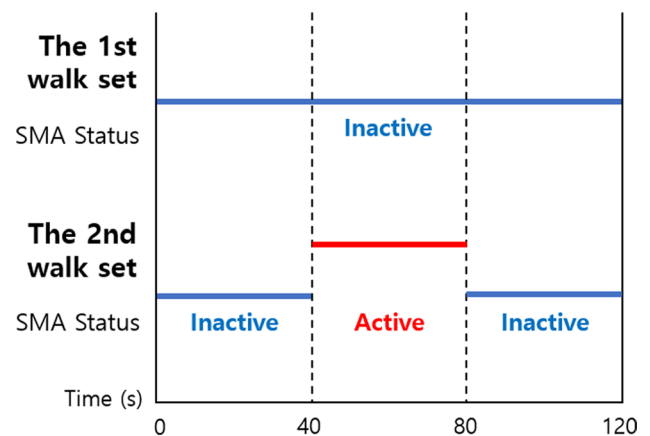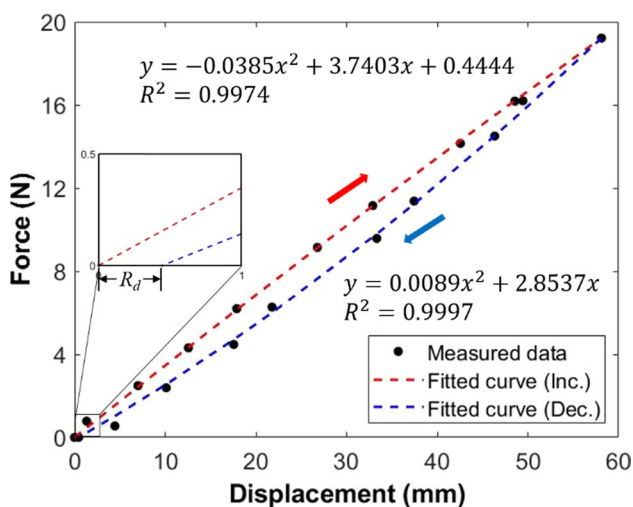
Fig. 13 Flow of the experiment protocol

Table 4 SMA actuator test results at input voltages of 12 V and 24 V

SMA actuator input voltage	12 V	24 V
Length change under 19.6 N (mm)	60	58
Surface temperature of SMA spring (°C)	96	227
Outside temperature of insulation cover (°C)	67	137
Contraction time (s)	23	1.7

fully at an input voltage of 24 V was found to be only 7.4% of the time required for the complete contraction of the SMA actuator at an input voltage of 12 V. Because one of the most important parameters of the SMA actuator for AFO operation is its contraction time, we decided to perform the subsequent tests with the SMA actuator at an input voltage of 24 V. For reference, the average power consumption at input voltages of 12 V and 24 V was 35.1 W and 128.8 W, respectively.

As shown in Table 4, the contraction time of a SMA actuator is inversely proportional to the input voltage but the temperature of SMA springs increases proportionally to the input voltage. To overcome the low efficiency and slow actuating frequency of SMA, a cooling system would be needed. However, in this study, the final design of SMA actuators excluded a cooling system but bias springs in consideration of the increased weight and volume when adding fans.

Figure 15 shows the hysteresis curve of the SMA actuator at an input voltage of 24 V, which is based on the average of 10 repeated tests. The hysteresis curve was curve-fitted with a quadratic equation, and the corresponding equations were $y = 0.0089x^2 + 2.8537x$ and $y = -0.0385x^2 + 3.7403x + 0.4444$

with R^2 values of 0.9997 and 0.9974, respectively. The beginning and end of the hysteresis curves do not coincide. This phenomenon is called residual displacement (R_d) and occurs when the SMA material shrinks and does not fully recover its original length, which is 0.444 mm [36]. The coordinates (a, b) and (c, d) for installing the SMA actuator on the AFO were (93, 382) and (209, 0), respectively. The maximum assistive torque from the SMA actuator was calculated to be 1384.4 N mm at these coordinates. Also, the displacement of the SMA actuator was 28.5 mm and the expected moment arm (r') was 147.2 mm when the lower part of the AFO was pulled towards the shin by the target assisting angle of 8° in the neutral state.

3.2 Gait phase analysis

Figure 16 shows the results of the GC detected using the AO algorithm. Figure 16 (a) depicts the COPx (solid black line) input into the AO and the COPx (red dotted line) learned through the AO, where the change in the trend of the learning results matches the actual value relatively well. φ_1 estimated by the AO is presented in Fig. 16 (b) and approaches 2π from the fifth step after the start of the walk test.

Furthermore, the average value of φ_1 for the walk test of participant #1 is 6.064 ± 0.189 rad, and this value shows an error of $(-)0.219$ rad compared with the ideal GC of 2π, which is a satisfactory level of error of approximately 0.219 rad/$(2\pi) = 3.4\%$.

Fig. 15 Hysteresis curve of SMA actuator with an input voltage of 24 V
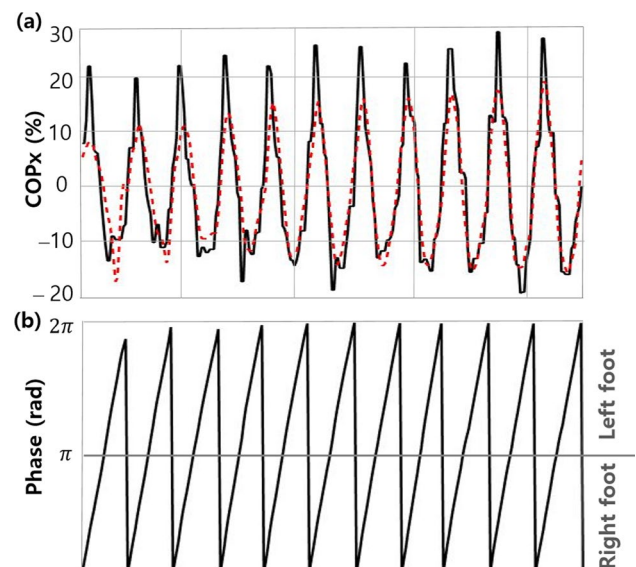
Fig. 16 Typical results of the continuous GC using the AO system for participant #1: **a** COPx. The black solid line indicates the input signal, and the red dashed line indicates the learned signal. **b** Gait phase in radians

3.3 Gait Aid Using the SMA-AFO

The change in ankle angle and the results of the statistical analysis for each participant with inactive and active SMA actuators are presented in Figs. 17, 18, and 19 and Table 5.

Figure 17 shows the average ankle angle (Figs. 17a, c, and e) and change in the average ankle angle (Figs. 17b, d, and f) for each participant with inactive and active SMA actuators. The average ankle angle and change in the average ankle angle of the three participants are depicted in Figs. 17g and h, respectively.

In Fig. 17(g), the ankle is lifted towards the shin and the ankle angle (θ) gradually increases from 60% of the GC, at which point power supply to the SMA actuator begins. It continues to increase until the next GC, and the ankle assist effect is maintained up to 10% of the target initial gait interval. Based on the data in Table 5, which presents the amount of change in the ankle angle measured in this experiment, the ankle angle can be increased by an average of 8.75° in the 0%–10% GC using the SMA-AFO. This value exceeds the target of 8° for the ankle assist angle set in this study, indicating that the device can produce sufficient walking assistance effect for patients whose toes touch the ground at the beginning of the GC owing to drop foot.

However, Fig. 17h shows that the position at which the increase in the ankle angle reaches its maximum value is approximately 80% of that of the GC. After turning off the power supplied to the SMA actuator at 10% of the next GC, the position at which the increase in the ankle angle reaches the lowest value is approximately 30% of the GC. In other words, the SMA actuator needs approximately 20% of the GC (approximately 0.8 s in terms of time) to reach a certain level of contraction of the SMA spring or to return to its original position depending on the supply of power.

In Fig. 17h, the change in ankle angle continuously decreases in the 0%–10% section of the GC, although the SMA actuator is supplied with power. This decrease occurs because the forefoot gradually descends towards the ground after the initial contact, where it touches the ground, progressing to a flat foot, and the ankle angle approaches the neutral state. In addition, a valley curve is observed in the 90% section of the GC in Fig. 17h, which may have been attributed to the unique ankle movement of Participant #1, as shown in Fig. 17a.

Based on 30%–60% of the GC in Fig. 17h, the ankle is lifted towards the shin by an average of 2°, even without the power supply to the SMA actuators. This feature could be interpreted as the result of pulling the lower part of the AFO, even in the section in which the power supply was cut off, because of the residual displacement phenomenon of the SMA, as shown in Fig. 15.

On the contrary, according to Wiszomirska et al., the ankle angle of patients with drop foot was –15.19 °± 3.1° in the 60%–100% GC range, and the ROM was limited by approximately 4.62° compared with that of healthy adults (–19.81 °± 0.9°) [20]. In Fig. 17h, sufficient changes in the ankle angle can be observed in 60%–100% of the GC, which is the heating section of the SMA actuator. Therefore, if the SMA-AFO is used, a walking aid effect can be obtained for patients with drop foot, even in the corresponding section.

Figure 18 provides a graph of Fig. 17g together with the ankle angle data at slow cadence obtained by Winter et al. [37]. Based on the state (SMA, inactive) of the SMA actuator in Fig. 18a, at 0% GC, the ankle droops towards the ground because of the mimicked gait pattern of the drop foot. Consequently, the forefoot touches the ground first during the LR thereby increasing the ankle angle. In MS, the ankle angle continuously increases as the sole becomes parallel to the ground in the range of 10%–30% of the GC. In other words, when reproducing the GC of P-F-P-S that mimics the gait pattern of drop foot, as the gait progresses, duration of the F section, where the right instep gets close to the shin, increases until the weight is completely transferred to the right foot fitted with the SMA-AFO and the left foot can be released, delaying the peak of the ankle angle. Thus, the maximum ankle angle appears approximately 42.6% of the way through the GC, corresponding to the end of the terminal stance (TS) in the slow gait of healthy adults, whereas the maximum ankle angle appears at approximately 64.8% of the GC, which is the initial stage of the initial swing after passing the pre-swing in the GC with inactive SMA actuators in this experiment. Previous studies have reported that changes in ankle angle are affected by walking speed [38, 39]. In the study by Schwartz et al. [38], the dimensionless gait speed was obtained using the gait speed and leg length of the participants, as shown in Eq. (14), and the results of examining the effect of the ankle angle according to gait speed were provided:

$$v^* = \frac{v}{\sqrt{g \cdot \text{leg length}}}. \tag{14}$$

In Fig. 18b, the point at which the maximum ankle angle appears is delayed as the dimensionless walking speed decreases. In other words, when the gait speed in this study is converted into a dimensionless gait speed, the result is 0.051 (v^*), which is the slowest gait speed among the data. Additionally, the maximum ankle angle appears at the latest time, which is consistent with the claim made by Schwartz et al. [38]. Therefore, this feature may have been due to the effect of the drop foot mimicking the gait and the effect of slow walking speed being integrated, as described above. With active SMA actuators, the point at which the maximum
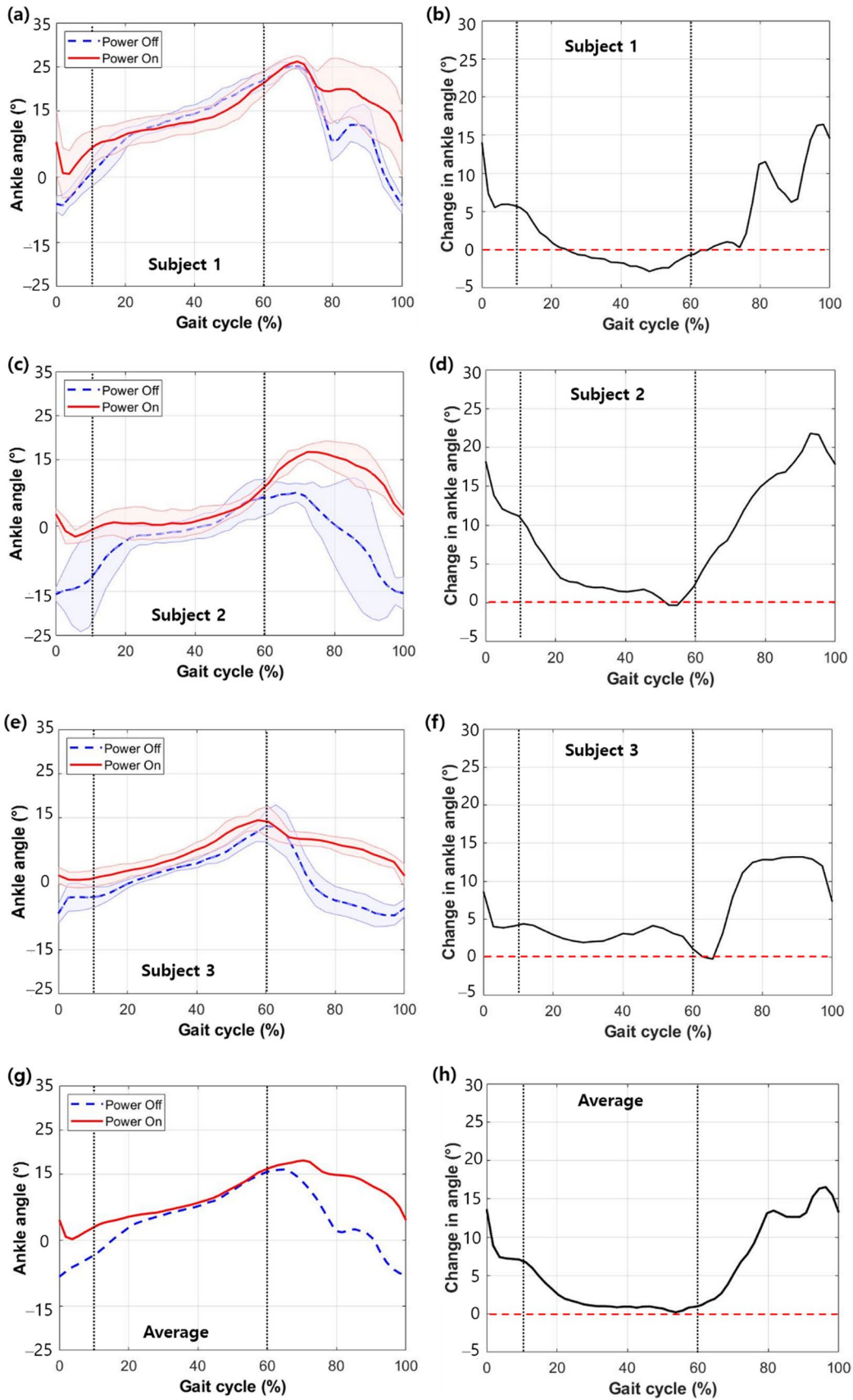
◀**Fig. 17** Ankle angles with the foot assistant on and off and the corresponding ankle changes of each participant. Red line: foot assistant on. Blue line: foot assistant off. The shaded areas represent the variance. **a** Ankle angle of participant #1, **b** change in the ankle angle of participant #1, **c** ankle angle of participant #2, **d** change in the ankle angle of participant #2, **e** ankle angle of participant #3, **f** change in the ankle angle of participant #3, **g** average ankle angle of the three participants, and **h** average change in the ankle angle of the three participants
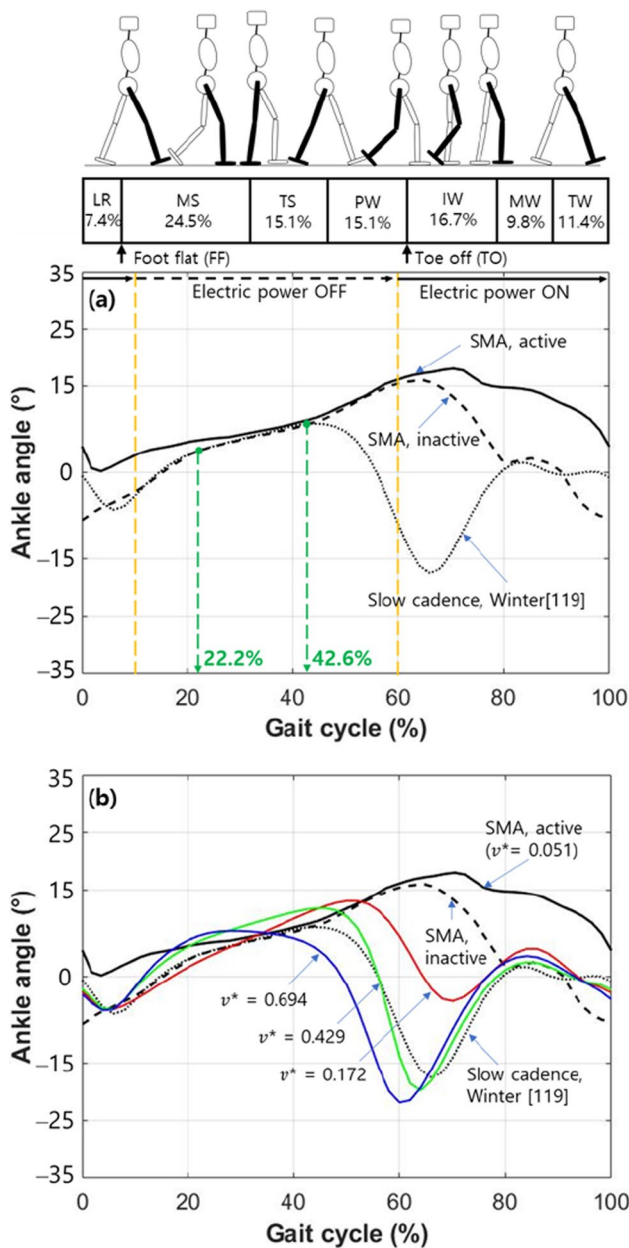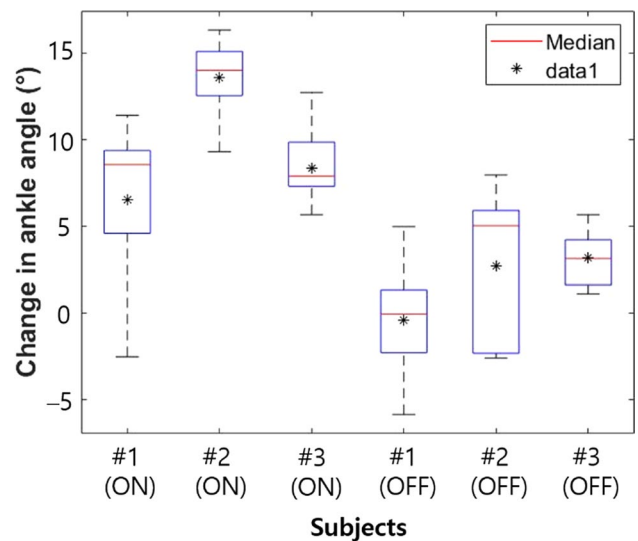

Fig. 19 Boxplots of five subjects with the foot assistant on and off

ankle angle appears is delayed more than that with inactive SMA actuators. A possible explanation of this finding is that the lower part of the AFO is pulled towards the shin and interferes with plantarflexion (PF) when the SMA actuators are active.

The change in the ankle angle caused by PF after achieving the maximum ankle angle is 26.04° and 23.81° for the slow cadence in the study by Winter et al. [37] and the inactive SMA actuator, respectively, showing a difference of 2.23°. Overall, the ankle angle change in the walk test with the developed SMA-AFO in an inactive state involves the ankle being pulled more by 7.52° in the DF direction and the ankle being lowered by 9.75° less in the PF direction. A possible explanation for this experimental result is the combination of the imitated gait pattern of the drop foot and the constrained ankle movement by the SMA-AFO and bias springs, which interferes with the PF, unlike the gait pattern of healthy adults.

However, the ankle angle of slow cadence in the study by Winter et al. is quite similar to that of inactive SMA actuator case in this study in the 22.2%–42.6% section of the GC corresponding to the MS and TS. Owing to the effect of the sole contacting the ground, there appeared to be little difference in the ankle angle, as it was the least affected by the gait change according to the drop foot, mimicking normal gait.

Based on the statistical analysis results in Table 5, the change in ankle angle is significant for all three participants in the entire GC, including when the power is off (0%–10% and 60%–100% of the GC) and on (10%–60%) (p = 0.000).

Fig. 18 Comparison of the variations in the average ankle angle

Table 5 Change in the ankle angle with the foot assistant power on and off

Participant No	Change in the ankle angle between power on/off (°)				P-value		
	0%–10% GC	60%–100% GC	ON*	Off*	0%–10% GC vs. Off	60%–100% GC vs. Off	ON vs. Off
1	7.45 (4.31)	6.22 (4.83)	6.48 (4.56)	–0.42 (3.03)	0.000	0.000	0.000
2	13.48 (7.14)	13.58 (3.64)	13.56 (2.60)	2.65 (4.79)	0.007	0.012	0.003
3	5.32 (2.92)	9.35 (3.03)	8.34 (2.10)	3.12 (1.53)	0.002	0.000	0.000
Overall	8.75 (4.23)	9.72 (3.69)	9.46 (3.67)	1.78 (1.92)	0.000	0.000	0.000

*On: 0%–10% of the GC and 60%–100% of the GC; **Off: 10%–60% of the GC

In Fig. 19, the change in the ankle angle shows a clear difference between the inactive and active SMA actuator cases for all participants. The above experimental data suggest that the walk test in this study was conducted without any problems.

4 Conclusion

In this study, we developed an SMA-AFO that can assist the ankle movement of patients with gait disorders and drop foot symptoms, conducted a walk test by making healthy adults mimic the gait pattern of patients with drop foot, and drew the following conclusions.

First, the weight of the SMA-AFO located on a lower extremity developed in this study was 1.24 kg, which is 13.8% lighter than the existing active-type AFO developed by Shorter et al. [10]; therefore, it can be easily used by patients with gait disorders or the elderly with weakened muscle strength. Second, the GC can be identified in real time using the COPx of the body in the left and right directions of the body during walking as input data for the AO algorithm. This method of calculating the GC can be applied to patients wearing an AFO or with a gait disorder and has the advantage of accurately determining the control point of the SMA. By accurately determining the GC in this manner, the current needed to operate the SMA actuator can be supplied to only 45.3% of the GC, thereby reducing the power consumption required for SMA operation and creating an ankle assist effect at a desired point in time. Third, when the SMA actuator was operated, the forefoot of the AFO was pulled towards the shin, and the ankle rotation angle increased by an average of 8.75°, confirming the ankle assistive effect. Therefore, the SMA-AFO and its control method devised in this study can be applied to patients with drop foot in the future.

In future studies, the operational efficiency of the SMA actuator and performance of the SMA-AFO system should be further investigated by conducting experiments on patients with drop foot.

Declarations

References

1. Jung, S. Y., Fekiri, C., Kim, H. C., & Lee, I. H. (2022). Development of plantar pressure distribution measurement shoe insole with built-in printed curved sensor structure. *International Journal of Precision Engineering and Manufacturing, 23*(5), 565–572. https://doi.org/10.1007/s12541-022-00637-y

2. Prakash, C., Kumar, R., & Mittal, N. (2018). Recent developments in human gait research: Parameters, approaches, applications, machine learning techniques, datasets and challenges. *Artificial Intelligence Review, 49*, 1–40. https://doi.org/10.1007/s10462-016-9514-6

3. Alexander, N. B. (1996). Gait disorders in older adults. *Journal of the American Geriatrics Society, 44*(4), 434–451. https://doi.org/10.1111/j.1532-5415.1996.tb06417.x

4. Sudarsky, L. (1990). Gait disorders in the elderly. *New England Journal of Medicine, 322*(20), 1441–1446. https://doi.org/10.1056/NEJM199005173222007

5. Schiemanck, S., Berenpas, F., van Swigchem, R., van den Munckhof, P., de Vries, J., Beelen, A., Nollet, F., & Geurts, A. C. (2015). Effects of implantable peroneal nerve stimulation on gait quality, energy expenditure, participation and user satisfaction in patients with post-stroke drop foot using an ankle-foot orthosis. *Restorative Neurology and Neuroscience, 33*(6), 795–807. https://doi.org/10.3233/RNN-150501

6. Carolus, A. E., Becker, M., Cuny, J., Smektala, R., Schmieder, K., & Brenke, C. (2019). The interdisciplinary management of foot drop. *Deutsches Ärzteblatt International, 116*(20), 347–354. https://doi.org/10.3238/arztebl.2019.0347

7. Alam, M., Choudhury, I. A., & Mamat, A. B. (2014). Mechanism and design analysis of articulated ankle foot orthoses for drop-foot. *The Scientific World Journal, 2014*, 867869. https://doi.org/10.1155/2014/867869

8. Blaya, J. A., & Herr, H. (2004). Adaptive control of a variable-impedance ankle-foot orthosis to assist drop-foot gait. *IEEE Transactions on neural systems and rehabilitation engineering, 12*(1), 24–31. https://doi.org/10.1109/TNSRE.2003.823266

9. Noël, M., Cantin, B., Lambert, S., Gosselin, C. M., & Bouyer, L. J. (2008). An electrohydraulic actuated ankle foot orthosis to generate force fields and to test proprioceptive reflexes during human walking. *IEEE Transactions on Neural Systems and Rehabilitation Engineering, 16*(4), 390–399.

10. Shorter, K. A., Kogler, G. F., Loth, E., Durfee, W. K., & Hsiao-Wecksler, E. T. (2011). A portable powered ankle-foot orthosis for rehabilitation. *Journal of Rehabilitation Research and Development, 48*(4), 459–472.

11. Choi, H. S., Lee, C. H., & Baek, Y. S. (2020). Design and validation of a two-degree-of-freedom powered ankle-foot orthosis with two pneumatic artificial muscles. *Mechatronics, 72*, 102469.

12. Waters, R. L., & Mulroy, S. (1999). The energy expenditure of normal and pathologic gait. *Gait & Posture, 9*(3), 207–231. https://doi.org/10.1016/S0966-6362(99)00009-0

13. Moltedo, M., Baček, T., Verstraten, T., Rodriguez-Guerrero, C., Vanderborght, B., & Lefeber, D. (2018). Powered ankle-foot orthoses: The effects of the assistance on healthy and impaired users while walking. *Journal of neuroengineering and rehabilitation, 15*(1), 1–25.

14. Al-Fahaam, H., Davis, S., & Nefti-Meziani, S. (2016). Wrist rehabilitation exoskeleton robot based on pneumatic soft actuators. In *2016 International Conference for Students on Applied Engineering (ICSAE),* Newcastle Upon Tyne, UK, pp. 491–496. https://doi.org/10.1109/ICSAE.2016.7810241

15. Nespoli, A., Besseghini, S., Pittaccio, S., Villa, E., & Viscuso, S. (2010). The high potential of shape memory alloys in developing miniature mechanical devices: A review on shape memory alloy mini-actuators. *Sensors and Actuators A: Physical, 158*(1), 149–160. https://doi.org/10.1016/j.sna.2009.12.020

16. Pittaccio, S., Viscuso, S., Rossini, M., Magoni, L., Pirovano, S., Villa, E., & Molteni, F. (2009). SHADE: A shape-memory-activated device promoting ankle dorsiflexion. *Journal of materials engineering and performance, 18*, 824–830.

17. Zhang, J., & Yin, Y. (2012). SMA-based bionic integration design of self-sensor–actuator-structure for artificial skeletal muscle. *Sensors and Actuators A: Physical, 181*, 94–102.

18. Deberg, L., Taheri Andani, M., Hosseinipour, M., & Elahinia, M. (2014). An SMA passive ankle foot orthosis: Design, modeling, and experimental evaluation. *Smart Materials Research, 2014*, 11.

19. Agostini, V., Balestra, G., & Knaflitz, M. (2013). Segmentation and classification of GCs. *IEEE Transactions on Neural Systems and Rehabilitation Engineering, 22*(5), 946–952. https://doi.org/10.1109/TNSRE.2013.2291907

20. Wiszomirska, I., Błażkiewicz, M., Kaczmarczyk, K., Brzuszkiewicz-Kuźmicka, G., & Wit, A. (2017). Effect of drop foot on spatiotemporal, kinematic, and kinetic parameters during gait. *Applied Bionics and Biomechanics, 2017*, 3595461. https://doi.org/10.1155/2017/3595461

21. Błażkiewicz, M., Wiszomirska, I., Kaczmarczyk, K., Brzuszkiewicz-Kuźmicka, G., & Wit, A. (2017). Mechanisms of compensation in the gait of patients with drop foot. *Clinical Biomechanics (Bristol, Avon), 42*, 14–19. https://doi.org/10.1016/j.clinbiomech.2016.12.014

22. Park, C. H., Choi, K. J., & Son, Y. S. (2019). Shape memory alloy-based spring bundle actuator controlled by water temperature. *IEEE/ASME Transactions on Mechatronics, 24*(4), 1798–1807. https://doi.org/10.1109/TMECH.2019.2928881

23. Jeong, J., Park, C. H., & Kyung, K. U. (2020, May). Modeling and analysis of SMA actuator embedded in stretchable coolant vascular pursuing artificial muscles. *In 2020 IEEE International Conference on Robotics and Automation (ICRA)*, Paris, France, 5641–5646. https://doi.org/10.1109/ICRA40945.2020.9197090

24. Park, C. H., & Son, Y. S. (2017). SMA spring-based artificial muscle actuated by hot and cool water using faucet-like valve. In *SPIE Smart Structures and Materials + Nondestructive Evaluation and Health Monitoring 2017,* Portland, OR, 10164, 165–174. https://doi.org/10.1117/12.2257467

25. Paredes, M., Sartor, M., & Masclet, C. (2001). An optimization process for extension spring design. *Computer methods in applied mechanics and engineering, 191*(8–10), 783–797. https://doi.org/10.1016/S0045-7825(01)00289-4

26. Park, S. J., Kim, U., & Park, C. H. (2020). A novel fabric muscle based on shape memory alloy springs. *Soft Robotics, 7*(3), 321–331. https://doi.org/10.1089/soro.2018.0107

27. Investigation of Korean body size. Retrieved 07 07, 2020, from https://sizekorea.kr/ (2003).

28. National Health Insurance press release (2017): Four out of five stroke patients are over 60 years old. Retrieved MM DD, YYY, from https://www.nhis.or.kr/nhis/together/wbhaea01600m01.do?mode=view&articleNo=123338&article.offset=0&articleLimit=10&srSearchVal=60%EC%84%B8+%EC%9D%B4%EC%83%81

29. Kim, G. T., Lee, M., Kim, Y., & Kong, K. (2023). Robust gait event detection based on the kinematic characteristics of a single lower extremity. *International Journal of Precision Engineering and Manufacturing.* https://doi.org/10.1007/s12541-023-00807-6

30. Yan, T., Parri, A., Ruiz Garate, V., Cempini, M., Ronsse, R., & Vitiello, N. (2017). An oscillator-based smooth real-time estimate of gait phase for wearable robotics. *Autonomous Robots, 41*, 759–774. https://doi.org/10.1007/s10514-016-9566-0

31. Park, J. S., & Kim, C. H. (2022). Ground-reaction-force-based gait analysis and its application to gait disorder assessment: New indices for quantifying walking behavior. *Sensors, 22*(19), 7558. https://doi.org/10.3390/s22197558

32. Park, J. S., Lee, C. M., Koo, S.-M., & Kim, C. H. (2020). Gait phase detection using force sensing resistors. *IEEE Sensors Journal, 20*(12), 6516–6523. https://doi.org/10.1109/JSEN.2020.2975790

33. Bogataj, U., Gros, N., Kljajić, M., Aćimović, R., & Maležič, M. (1995). The rehabilitation of gait in patients with hemiplegia: A comparison between conventional therapy and multichannel functional electrical stimulation therapy. *Physical therapy, 75*(6), 490–502. https://doi.org/10.1093/ptj/75.6.490

34. Karunakaran, K. K., Pilkar, R., Ehrenberg, N., Bentley, K. S., Cheng, J., & Nolan, K. J. (2019). Kinematic and functional gait changes after the utilization of a foot drop stimulator in pediatrics.

Frontiers in Neuroscience, 13, 732. https://doi.org/10.3389/fnins.2019.00732

35. Ramachandran, K. M., & Tsokos, C. P. (2020). *Mathematical statistics with applications in R.* Academic Press.

36. Chowdhury, M. A., Rahmzadeh, A., & Alam, M. S. (2019). Improving the seismic performance of post-tensioned self-centering connections using SMA angles or end plates with SMA bolts. *Smart Materials and Structures, 28*(7), 075044. https://doi.org/10.1088/1361-665X/ab1ce6

37. Winter, D. A. (1991). *Biomechanics and motor control of human gait: normal, elderly and pathological.* Transport Research Laboratory.

38. Schwartz, M. H., Rozumalski, A., & Trost, J. P. (2008). The effect of walking speed on the gait of typically developing children. *Journal of Biomechanics, 41*(8), 1639–1650. https://doi.org/10.1016/j.jbiomech.2008.03.015

39. Ong, C. F., Geijtenbeek, T., Hicks, J. L., & Delp, S. L. (2019). Predicting gait adaptations due to ankle plantarflexor muscle weakness and contracture using physics-based musculoskeletal simulations. *PLoS Computational Biology, 15*(10), e1006993. https://doi.org/10.1371/journal.pcbi.1006993

Bohyun Lee received the B.S. degree in biomedical engineering from University of California-Davis, Davis, CA, in 2017, and the M.S. degree in mechanical engineering from Korea University, Seoul, South Korea, in 2022. Her research interests include biosignal analysis, gait analysis, and prognostics and health management.

Ji Su Park received the B.Eng. degree in mechanical and system design engineering from Hongik University, South Korea, in 2013, and the Ph.D. degree in electronic materials engineering from in Kwangwoon University, Seoul, Korea in 2021. His research interests include signal analysis, human–robot interaction, prognostics and health management, pattern recognition.

Shinsuk Park received the B.S. and M.S. degrees in mechanical design and production engineering from Seoul National University, Seoul, Korea, in 1989 and 1991, respectively, and the Ph.D. degree in mechanical engineering from the Massachusetts Institute of Technology, Cambridge, in 1999. From 2000 to 2002, he was a Postdoctoral Research Fellow with the Biorobotics Laboratory, Harvard University, Cambridge. He is currently a Professor with the Department of Mechanical Engineering, Korea University, Seoul. His research interests include dynamics systems and control and their applications to human–machine interface design and biomedical engineering problems.

Choong Hyun Kim received the Ph.D. degree in mechanical engineering from Hanyang University, Seoul, Korea, in 2001. In 2011 he joined the center for bionics of Korea Institute of Science and Technology (KIST), Seoul. His current research interests include gait analysis, gait rehabilitation, fall detection as well as machine element design.